

# Liquid-Assisted Mechanochemical Synthesis of LiI-Doped Sulfide Glass Electrolyte

Seyed Milad Hosseini, Alberto Varzi,\* Tomoyuki Tsujimura, Yuichi Aihara, and Stefano Passerini\*

Inorganic solid electrolytes (ISEs) gain tremendous attention during the past decade for application in energy storage. Among different classes of ISEs, sulfides are particularly appealing due to their higher ionic conductivity, ductility, and lower density compared with oxides. However, most of the preparation methods proposed so far require either the time-consuming mechanical ball-milling process or the energy-consuming high-temperature solid-state reaction. Herein, a new and fast liquid-assisted approach to synthesize LiI-doped glassy  $\text{Li}_2\text{S-P}_2\text{S}_5$  (LPS) with excellent electrochemical and morphological features is reported. The obtained solid electrolyte offers an ionic conductivity of  $1.2 \text{ mS cm}^{-1}$  at room temperature and establishes a rather stable interphase with lithium. These enable rather high critical current densities (up to  $1 \text{ mA cm}^{-2}$ ), as well as enhanced cathode active material utilization in solid-state lithium metal cells.

be overcome.<sup>[3]</sup> Among the available classes of inorganic solid electrolytes (ISEs), sulfide-based electrolytes have so far demonstrated the highest ionic conductivities (up to  $25 \text{ mS cm}^{-1}$ ).<sup>[4]</sup> In fact, compared with oxides,  $\text{Li}^+$  mobility in sulfides is promoted by a lower electronegativity of sulfur, which translates in lower binding energy to  $\text{Li}^+$  ions.<sup>[5]</sup> In addition, sulfur has a large atomic radius, creating larger channels for  $\text{Li}^+$  ion conduction in the solid structure.<sup>[6]</sup>

One of the most studied sulfide-based solid electrolytes is the glassy  $\text{Li}_2\text{S-P}_2\text{S}_5$  (LPS) with room temperature ionic conductivities up to  $0.28 \text{ mS cm}^{-1}$  depending on the stoichiometry, crystal structure, and synthesis method.<sup>[5,7]</sup> However, these solid ion

## 1. Introduction


During the past decades, most of the research efforts in the lithium battery field were focused on lithium-ion batteries (LIBs) using liquid electrolytes.<sup>[1]</sup> Despite the benefits of liquid electrolytes such as high ionic conductivity at room temperature and easy wetting of the electrodes, they suffer from low  $\text{Li}^+$  transference number, limited electrochemical and thermal stability resulting in gas evolution, and, most importantly, poor safety.<sup>[2]</sup> By replacing the liquid electrolyte with a solid conductor, some of the aforementioned issue of the current state of the art LIB may

conductors have a limited electrochemical stability window.<sup>[8]</sup> The addition of Li halides to LPS is known to increase the free volume in the structure, resulting in the increase in ionic conductivity and electrochemical stability.<sup>[9]</sup> In fact, various papers on LiI-doped LPS (LPSI) report ionic conductivities up to  $1 \text{ mS cm}^{-2}$ .<sup>[10]</sup> Among the possible dopants, iodide also improves the compatibility of the solid electrolyte with lithium metal,<sup>[10d]</sup> which is of foremost importance for solid-state-batteries (SSB) applications. Despite these appealing features, sulfides are highly reactive toward humidity; therefore, they must be synthesized under an inert atmosphere. It is worth mentioning that replacing phosphorous with antimony can decrease the reactivity of the sulfide-based solid electrolytes toward humidity. However, the ionic conductivity is substantially lowered.<sup>[11]</sup> So far, the most common route to synthesize glassy sulfidic ISEs are melt quenching and ball-milling.<sup>[5,7c,12]</sup> The melt quenching method is widely used to obtain glassy solid electrolytes; however, the high-temperature required increases the risk of undesirable side reactions due to the interaction between the reagents and reaction vessel. Moreover, the loss of the reactants by evaporation is often observed during the synthesis, which appears as condensation on the surface of the vessel after cooling.<sup>[7c]</sup> In contrast, ball-milling can be performed at room temperature, eliminating the necessity of troublesome high temperature and quenching operations.<sup>[5]</sup> In fact, most sulfide glass conductors can be produced by ball-milling, and crystalline phases can be obtained by a consecutive annealing step. As drawback, the ball-milling method is greatly time-consuming. Due to the ductility and softness of the sulfides, the reactants tend to agglomerate in the mill jar and, consequently, slow down the reaction. To break the agglomerates apart, opening of the reaction vessel is regularly

S. M. Hosseini, A. Varzi, S. Passerini  
Helmholtz Institute Ulm (HIU)  
Helmholtzstrasse 11, 89081 Ulm, Germany

S. M. Hosseini, A. Varzi, S. Passerini  
Karlsruhe Institute of Technology (KIT)  
P.O. Box 3640, 76021 Karlsruhe, Germany  
E-mail: alberto.varzi@kit.edu; stefano.passerini@kit.edu

T. Tsujimura, Y. Aihara  
Samsung R&D Institute Japan  
Senbanishi 2-1-11, Minoh, Osaka, Japan

 The ORCID identification number(s) for the author(s) of this article can be found under <https://doi.org/10.1002/ente.202100385>.

© 2021 The Authors. Energy Technology published by Wiley-VCH GmbH. This is an open access article under the terms of the Creative Commons Attribution-NonCommercial-NoDerivs License, which permits use and distribution in any medium, provided the original work is properly cited, the use is non-commercial and no modifications or adaptations are made.

DOI: 10.1002/ente.202100385

required. This increases the synthesis time as well as the probability of contamination for the resulting solid electrolyte. Moreover, the homogeneity and reproducibility are not always guaranteed in ball-milling synthesis, due to the variations of the mechanical shier and the applied energy.

Considering these issues, the synthesis of glassy sulfidic electrolytes in liquid can be an effective method to shorten reaction time and produce homogenous products.<sup>[7c]</sup> The liquids suitable for the synthesis of sulfide solid electrolytes are restricted to nonpolar or less polar aprotic solvents due to the high reactivity of the precursors toward polar solvents.<sup>[13]</sup> Several liquid media have been used so far to synthesize LPSI such as ACN,<sup>[10a]</sup> heptane,<sup>[10c]</sup> ethyl propionate (EP),<sup>[14]</sup> and 1,2-dimethoxyethane (DME).<sup>[10b,15]</sup> The use of the aforementioned solvents requires long time to dissolve the precursors. Also, the procedure usually includes several steps including drying at elevated temperature and under vacuum, consequently increasing the chance of contamination and errors during the synthesis (see Table S1, Supporting Information, for a detailed summary of previous publications).

In this work, we report a novel reaction method to obtaining glassy 35LiI-65(3Li<sub>2</sub>S-1P<sub>2</sub>S<sub>5</sub>) solid electrolyte. The mechanochemical synthesis is aided by the addition of benzene as liquid medium, which enables shorter synthesis time and yields a highly ionic conductive solid electrolyte. Benzene has a lower dielectric constant compared with the solvents previously mentioned, resulting in the dispersion of the precursors rather than their dissolution; therefore, enhancing the mechanochemical process. In addition, as almost all of the benzene quickly evaporates at room temperature with negligible (<1 wt%) trace left in the solid electrolyte powder, no additional drying of the resulting product is required. It is worth mentioning that the liquid-to-solid ratio in this work is considerably smaller than for other liquid-assisted and/or liquid synthesis previously reported (1.5 vs 25–50 mL g<sup>-1</sup>).<sup>[16]</sup> The low amount of benzene used in this work decreases the safety risks associated with solvents commonly used for the liquid-phase synthesis of SEs. In this specific case, the low amount of benzene used is also motivated by its harmful nature. The solid electrolyte powder shows a particle size lower than the equivalent material made via dry ball-milling. The ionic conductivity at room temperature is 1.2 mS cm<sup>-1</sup>, which is comparable with the highest values previously reported.<sup>[10a,10b,14b]</sup> In addition, the solid electrolyte obtained via liquid method shows critical current density up to 0.8 mA cm<sup>-2</sup>, which is higher than that of the same compound synthesized via the dry method. Finally, it is shown that Li/LPSI/CuS all-solid-state cells using the solid electrolyte made via the liquid-assisted route outperform those with SE obtained via the dry method, due to the smaller particle size of the former material.

## 2. Results and Discussion

To optimize the reaction conditions, the impact of wet ball-milling time on the LPSI performance was initially evaluated. The X-ray diffraction (XRD) investigation of the LPSIs prepared by increasingly long treatments is shown in Figure 1a. It can be clearly seen that the XRD pattern of the solid electrolyte resulting by milling the precursors for 27 h in benzene (Wet-27) is very

similar to that of the material made by dry milling for the same time (Dry-27). Note that, despite the same ball-milling time, the overall time required for the dry procedure amounts to twice that needed for the wet process, due to the agglomeration of the reactants inside the jars when no liquid is present, which regularly requires opening of the reaction vessel to break the agglomerates apart. They both evidence an essentially amorphous structure typical of glassy compounds. However, two broad peaks centered at 21.1° and 28° (2 $\theta$ ) are detected (shaded regions in Figure 1a), which are characteristic of crystalline Li<sub>4</sub>PS<sub>4</sub>I.<sup>[10b]</sup> These peaks further evolve, along with the other characteristic diffraction peaks of Li<sub>4</sub>PS<sub>4</sub>I, upon annealing after the wet synthesis (see Figure S1, Supporting Information). Nevertheless, as the properties of the crystalline samples were found to be inferior to the glassy electrolyte, this path was not followed further (see Figure S2, Supporting Information). Additional reflections in Figure 1a can also be detected at 25.6°, 29.6°, 42.4°, and 50.2° (2 $\theta$ ), testifying some residual, unreacted LiI. On the contrary, the Li<sub>2</sub>S is completely reacted with P<sub>2</sub>S<sub>5</sub>, as evident by the disappearance of the diffraction peak of Li<sub>2</sub>S at 27.5° (2 $\theta$ ) between 21 and 27 h. A further confirmation comes from the Raman spectra shown in Figure 1b. The complete reaction of P<sub>2</sub>S<sub>5</sub> and Li<sub>2</sub>S to form PS<sub>4</sub> tetrahedra is indeed testified by the peak at 420 cm<sup>-1</sup>, which can be ascribed to the stretching of the PS<sub>4</sub> anion.<sup>[17]</sup> The absence of additional features in this region indicates the lack of other impurities, such as P<sub>2</sub>S<sub>7</sub> (387 cm<sup>-1</sup>) or P<sub>2</sub>S<sub>6</sub> (405 cm<sup>-1</sup>), which are observed when the reaction time is not sufficient to complete the reaction.<sup>[17a]</sup> In addition, it is worth mentioning that only a minimum amount of benzene is left in the solid electrolyte (i.e., about 1 wt% according to TGA-MS measurements). Such benzene trace is most likely trapped in the solid electrolyte structure, as it could not be removed even applying ultrahigh vacuum (Figure S3, Supporting Information). Therefore, it is not expected to impact the interfacial properties of the electrolyte such as, e.g., the stability toward Li metal.

The ionic conductivity of the solid electrolytes was determined via electrochemical impedance spectroscopy (EIS). Independent from the wet and dry preparation methods, Dry-27 and Wet-27 show the Arrhenius-type temperature dependence with high ionic conductivity at room temperature and an activation energy of 33.3 kJ mol<sup>-1</sup> (Figure 1c). The ionic conductivity increases twofold as the milling time of the wet process increases from 11 to 27 h, i.e., when the reaction is completed and the more phase-pure solid electrolyte with only PS<sub>4</sub> tetrahedra is formed. It is worth mentioning that stainless steel is commonly used for measuring ionic conductivity of all of the samples; therefore, the values in Figure 1c are lower than the actual value of the ionic conductivity.<sup>[10e,18]</sup> Using a soft electronic conductor such as indium helps improving the contact between the SE pellet and the electrodes and, therefore, obtaining a more representative value of bulk ionic conductivity (see Figure S4a, Supporting Information).<sup>[19]</sup> The almost blocking character of In under the small amplitude AC signal (10 mV) used for the EIS measurements is confirmed by the behaviour comparable with that of stainless steel and carbon cloth electrodes (see Nyquist plots in Figure S4b, Supporting Information).

To understand the impact of the liquid on the solid electrolyte morphology, scanning electron microscopy (SEM) analysis of the obtained powders was performed (Figure 2). Both the wet and

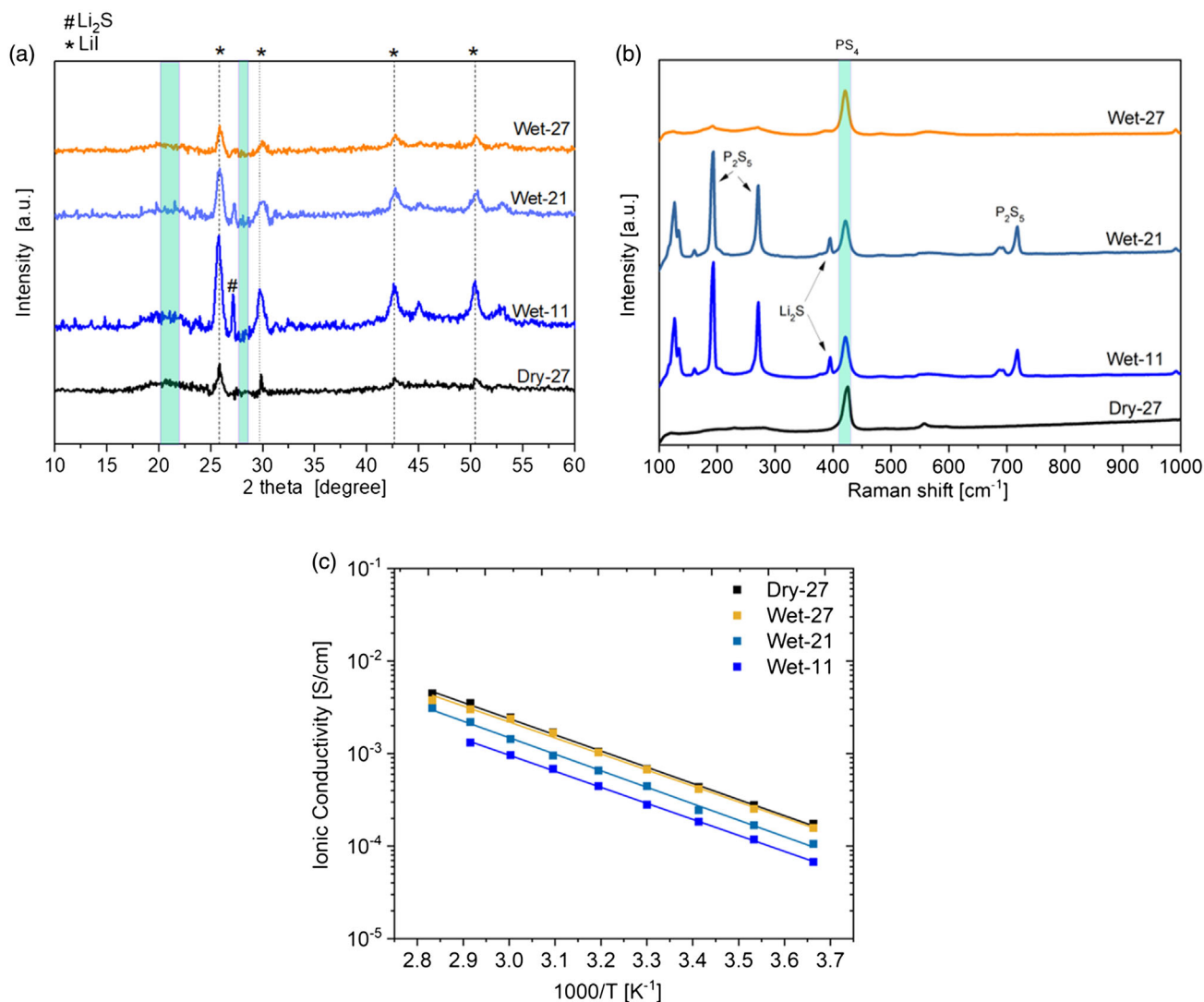


**Figure 1.** a) XRD patterns, b) Raman spectra, and c) temperature dependence ionic conductivity of  $\text{LiI-Li}_2\text{S-P}_2\text{S}_5$  solid electrolytes prepared via dry ball-milling for 27 h (black), wet ball-milling for 11 h (dark blue), 21 h (dull blue), and 27 h (yellow). Shaded areas in panel (a) and (b) show the characteristics of  $\text{Li}_4\text{PS}_4\text{I}$  crystal structure and  $\text{PS}_4$  anion, respectively.

the dry preparation methods result in spherical particles with diameter of few  $\mu\text{m}$  (2–10  $\mu\text{m}$ ) covered by bright submicrometric islands (Figure 2a,b). When compared with other LPS solid electrolytes from various references, and the  $\text{LiI}$  powder, these islands could be potentially composed by the  $\text{LiI}$  residues detected by XRD (see Figure S5, Supporting Information).<sup>[7b,20]</sup> Unfortunately, they appeared very sensitive to the electron beam, which causes the islands to vanish at high magnification (i.e., high energy electron beam) hindering their elemental analysis by energy-dispersive X-ray spectroscopy (EDX).

However, the main difference between the two synthesis methods is already evident at lower magnification (Figure 2c,d). Due to the high ductility and softness, LPSI easily forms agglomerates with coral-like shapes. However, the solid electrolyte prepared via the wet method shows a larger number of small

isolated particles with submicrometric size, which can be beneficial in terms of interface formation with the electrodes' active materials.<sup>[21]</sup>

To investigate the  $\text{Li}^+$  transport properties of LPSI, lithium stripping/plating tests of symmetric  $\text{Li/LPSI/Li}$  were conducted at 20 °C using stepwise increasing current densities. EIS measurements were also performed after each stripping and plating step.

The square-like overpotential profile recorded upon the lithium stripping/plating tests (Figure 3a) reveals the single-ion conductive behavior of the solid electrolytes. The wet LPSI appears to have improved interfacial properties, as indicated by the lower overvoltage at each current density. Also, the Wet-27 electrolyte offers a better performance toward lithium dendrite growth, standing plating at  $1 \text{ mA cm}^{-2}$  for 30 min before showing the typical fingerprint of dendrites formation (i.e., short circuiting),

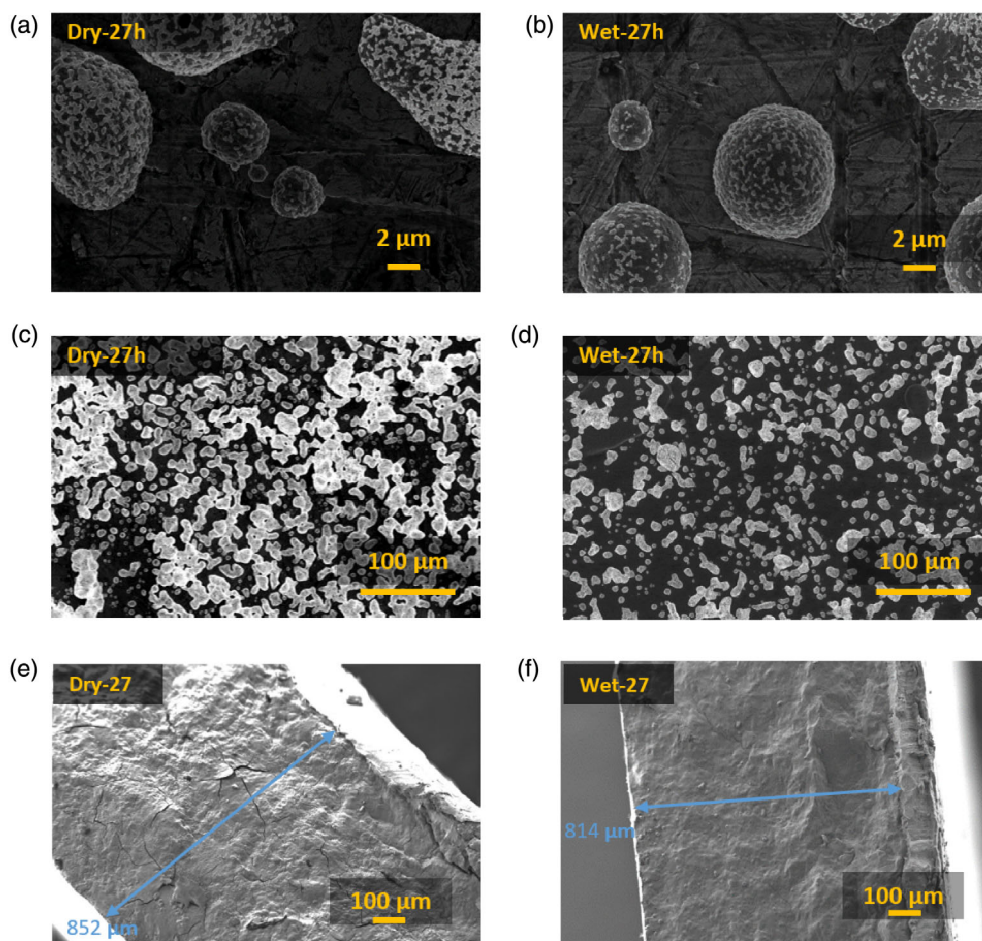


**Figure 2.** SEM images of LPSI solid electrolyte prepared via dry ball-milling for 27 h at a,c) different magnification, via wet method for 27 h at b,d) different magnification and e,f) the cross section of their pellets.

whereas the dry LPSI fails to operate already at a current density of  $0.8 \text{ mA cm}^{-2}$  due to Li dendrite formation (Figure 3a). Here, the slightly smaller particle size of Wet-27 can have the double advantage of 1) increasing the packing of the solid electrolyte layer and 2) establishing a better interface (larger contact area) with Li. In both cases, this will result in less voids (both in the SE bulk and at the electrode interface), which are known to be one of the main reasons for lithium dendrite formation.<sup>[22]</sup>

The EIS measurements of symmetric Li/LPSI/Li cells after one galvanostatic step are shown in Figure 3b. The impedance spectra of symmetric lithium metal cells incorporating Dry-27 and Wet-27 electrolytes show very similar shape, with an inductive tail at high frequency, a small semicircle in the kHz region, and a large semicircle in the mHz region (Figure 3b). These can be modelled with the equivalent circuit consisting of an inductor ( $L_1$ ), accounting for the high frequency inductive behavior of cabling, a resistance ( $R_0$ ) related to the bulk resistance of the solid electrolyte, and two parallel RC elements accounting for the processes occurring at the Li/LPSI interface. In particular, the high- and low-frequency RC elements are assigned to the  $\text{Li}^+$  transport through the passivation layer ( $R_1|\text{CPE}_1$ ) and the charge transfer process ( $R_2|\text{CPE}_2$ ), respectively (Figure 3b).<sup>[23]</sup>

From the EIS measurements and the fitting results, it is evident that Wet-27 electrolyte has lower bulk resistance. This is certainly due to the better packing of the small particles resulting in a thinner and more compact layer considering that the same mass of LPSI was used to prepare the symmetric lithium cells (Figure 3e, bottom panel). In fact, this is well evidenced by the cross-sectional SEM images of the two pellets (Figure 2e,f), showing several microcracks in the bulk of Dry-27, whereas less cracks are evident in the Wet-27 pellet. In addition, the resistance due to the electronic contact between solid electrolytes and electrodes influences the value of  $R_0$ . The different value of  $R_0$  obtained from EIS of symmetric cells with different electrodes is shown in Figure S4b, Supporting Information, and clearly shows the impact of the electrode/electrolyte contact on the value of the  $R_0$ . This latter can be another reason for the variation of the  $R_0$  upon stripping and plating of lithium because in each galvanostatic step higher amount of lithium is stripped or plated from lithium and can strongly influence the contact area.

The high-frequency resistance ( $R_1$ ), which is assigned to the passivation layer formed at the interphase with Li, is around  $1 \Omega$  and remains almost unchanged even after tests at current density of  $0.2 \text{ mA cm}^{-2}$  for both electrolytes (Figure 3e, middle panel).<sup>[23]</sup>



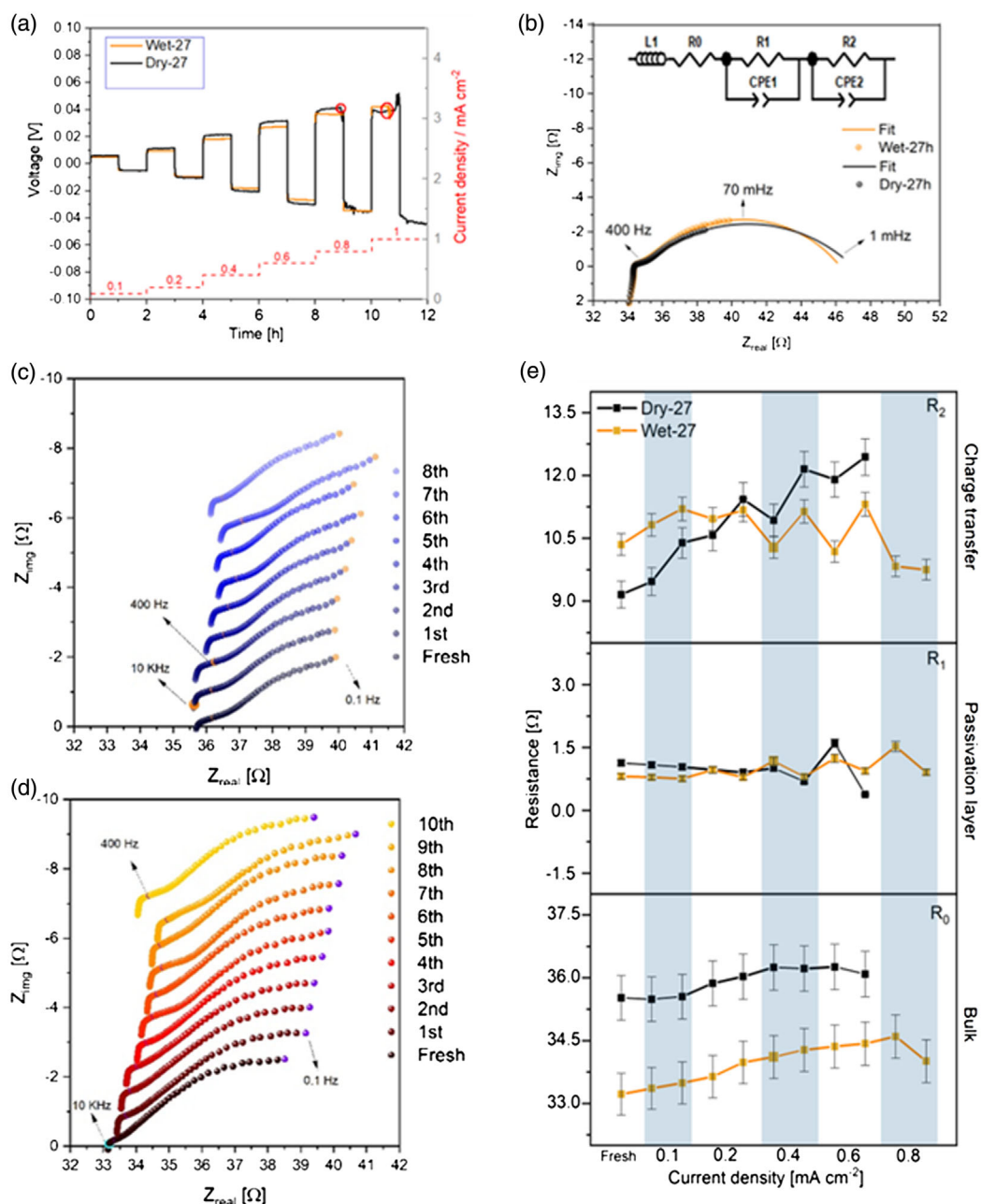


**Figure 3.** Characterization of Li/LPSI/Li symmetric cells using Wet-27 and Dry-27 electrolytes. All measurements were performed at 20 °C. a) Galvanostatic cycling at increasing current densities. b) EIS measurements after first current step (the equivalent circuit used for fitting the measurements and the fit results are also shown) and c,d) after each galvanostatic steps. e) Evolution of the bulk, low- and high-frequency resistance of the cells (the error bars, 1.5% for  $R_0$ , 3% for  $R_1$ , and 6% for  $R_2$ , are obtained from the fitting software).

This resistance fluctuates around 1 Ω as the current density increases. However, the Wet-27 electrolyte has smaller change in  $R_1$  compared with Dry-27 upon continuous cycling. The almost identical value of  $R_1$  for both solid electrolytes confirms that the 1 wt% leftover benzene does not have any detrimental reactivity toward lithium.

The charge transfer resistance ( $R_2$ ), which constitutes the main part of the total interfacial resistance ( $R_1 + R_2$ ), is stable around 11–12 Ω for the cell with Wet-27 electrolyte, whereas the cell with

Dry-27 electrolyte shows a continuous increase up to 12.5 Ω before it is short-circuited (Figure 3e, top panel).<sup>[24]</sup> The stability of the charge transfer resistance ( $R_2$ ) of Wet-27 upon prolonged plating and stripping of lithium supports for an improved contact between LPSI and lithium. In summary, the smaller average particle size of the Wet-27 solid electrolyte appears to be effective to form a more uniform interface with lithium metal and also a denser solid electrolyte layer, which are both crucial aspects to inhibit lithium dendrite penetration.<sup>[25]</sup>

Finally, the LPSIs were incorporated in solid-state cell using CuS as active material for the positive electrode. According to previous work, CuS-based electrodes can offer excellent performance in terms of reversible capacity and stability upon hundreds of cycles only when a large fraction of the positive electrode consists of the solid electrolyte (50 wt%).<sup>[26]</sup> Herein, however, we reduced the LPSI content in the positive electrode to 35 wt%, to get closer to the typical composition of a liquid electrolyte cell, in which the 30% porosity is filled by the liquid electrolyte, taking advantage of the small particles obtained via the liquid-assisted synthesis. It is worth mentioning that a lower fraction of SE in CuS composite cathodes can be achieved, as previously reported by Santhosha et al.<sup>[27]</sup> Herein, the cathode composites are not fully optimized, but we believe that the mass loading of the cathode active material can be certainly increased to take further advantage of the smaller SE particles obtained by the liquid-assisted synthesis. **Figure 4a** shows the capacity retention of Li/LPSI/CuS cells using the Wet-27 and Dry-27 materials in both the composite positive electrode and the solid electrolyte layer. The delivered capacity of the cell incorporating Wet-27 is higher at the first cycles compared with the Dry-27 cell. In addition, the delivered capacity is better retained upon cycling. Both

improvements certainly originate from the larger active material/solid electrolyte contact area granted by the finer Wet-27 particles, leading to higher active material utilization. Both cells display similar voltage profiles (Figure 4b, c), with a discharge plateau at 1.6 V due to conversion reaction of CuS to metallic Cu and a higher voltage plateau at 2.2 V, which is assigned to the reactivity of sulfur (generated upon cycling by the incomplete conversion to CuS).<sup>[26b]</sup> Interestingly, the redox activity of the solid electrolyte at higher potential (2.8 V) is not observed here.<sup>[17a]</sup> Compared with our previous work,<sup>[26b]</sup> this difference can only be associated with the lowest amount of solid electrolyte used here, but further investigations are needed to clarify this phenomenon.

It is also worth mentioning that the difference in delivered capacity by the Wet-27 and Dry-27 cells originates from the increase in the capacity at high voltage for Wet-27, whereas Dry-27 does show such behavior (see Figure S6, Supporting Information). The increased capacity at high voltage can be rooted to the better sulfur utilization originated from the only partially reversible conversion of CuS.<sup>[26b]</sup> The cell with Wet-27 shows very stable cycling performance, whereas the Dry-27 cell stops after 30 cycles due to the lithium dendrites and

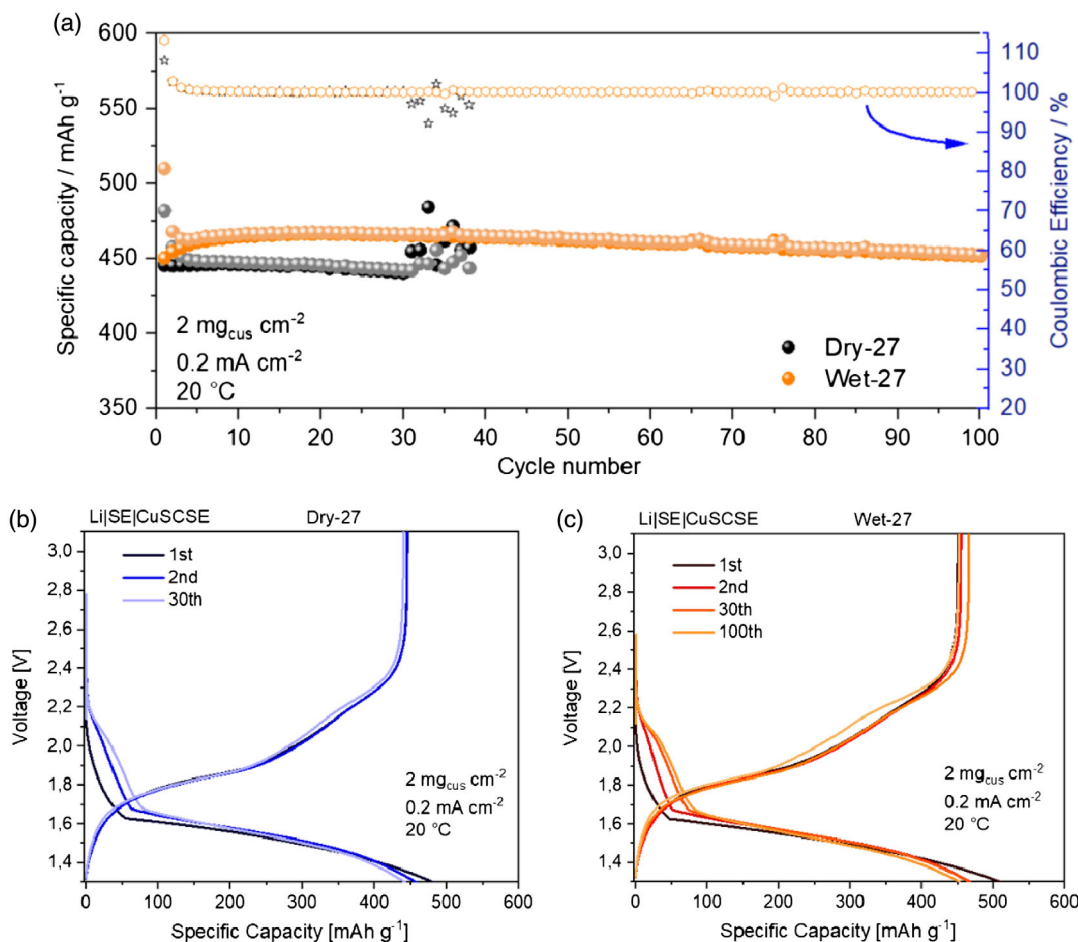


**Figure 4.** a) Delivered capacity and coulombic efficiency and b) selected voltage profiles of solid-state lithium metal cells, incorporating the (CuS-C-LPSI) composite cathodes and LPSI, upon galvanostatic cycling.

consequently the cell short circuits. This is again in accordance with the plating/stripping cycling and EIS measurements of symmetric Li/LPSI/Li cells, where the Wet-27 SE appears to form a more efficient interface with lithium due to the smaller particles, therefore resulting in lower local current densities; thus, lower chance of lithium dendritic growth.

### 3. Conclusion

In summary, LiI-doped sulfide glassy electrolytes were prepared by a simple liquid-assisted mechanochemical route requiring lower time and energy consumption compared with the common dry-milling methods. The prepared solid electrolyte offers an ionic conductivity of  $1.2 \text{ mS cm}^{-1}$  at room temperature with an activation energy of  $33.3 \text{ kJ mol}^{-1}$ . The liquid-assisted synthesis also yields smaller particles compared with the dry ball-milling approach, which are beneficial to the establishment of a better interface with lithium metal resulting in a smaller charge transfer resistance and higher critical current density. Even more importantly, the LPSI prepared via the wet method enhances the performance of Li/CuS solid-state batteries enabling higher delivered capacities, i.e., higher material utilization, and prolonged reversible cycling.

### 4. Experimental Section

LiI (Alfa Aesar, anhydrous, 99.95% metals basis),  $\text{Li}_2\text{S}$  (Albemarle, 99.9% metals basis), and  $\text{P}_2\text{S}_5$  (Sigma-Aldrich, 99%) were weighed with the molar ratios of 35LiI-65( $3\text{Li}_2\text{S}$ -1 $\text{P}_2\text{S}_5$ ), respectively, in total (2 g) and ground in an agate mortar for few minutes. The obtained mixture was transferred in a 45 mL zirconia jar with 10 g of 1 mm, seventeen 5 mm, and ten 1 cm zirconia balls. Benzene (3 mL) (Sigma-Aldrich, anhydrous 99.8%) was added in the jar and a clamping system was used to ensure the tightness of the jars. The mixture was ball-milled within a Pulverisette 4 (FRITSCH), with 380 rpm alternatively for 10 min of milling and 5 min of rest for 11–27 h of active milling. The jars transferred to an argon-filled glove box with special filters for solvents and let open in the glove box for few hours to evaporate the benzene. Finally, the solid electrolyte was collected from the jar and grounded in agate mortar prior to use for further work. The dry LSPI was received from SRJ Japan and was prepared with the same mechanochemical procedure only without any liquid previously reported.<sup>[26]</sup> The morphological and structural characterization was performed by field emission SEM (Zeiss LEO1550VP Gemini) and XRD (Bruker D8 Advance diffractometer equipped with a Cu K $\alpha$  source  $\lambda = 0.154 \text{ nm}$ ). An airtight, Ar-filled sample holder was used to transferring the samples from the glove box to the SEM chamber. For the XRD measurements, airtight sample holders were used to avoid sample degradation. Raman spectroscopy measurements were conducted in a confocal InVia Raman microspectrometer (Renishaw) with a 633 nm red laser and a 50 $\times$  objective lens. TGA was performed under  $\text{N}_2$  stream in a temperature range of 30–600 °C, with a constant heating rate of  $5^\circ\text{C min}^{-1}$  using Netzsch, TG 209 F1 Libra. For cell assembly, an in-house, two-electrode ( $\varnothing = 13 \text{ mm}$ ) cell (Torque cell) was used.<sup>[28]</sup> For the symmetric lithium cells, lithium metal disks (thickness = 30  $\mu\text{m}$ ,  $\varnothing 1.2 \text{ cm}$ ; Honjo Metal, Osaka) were used. About 200 mg of LiI- $\text{Li}_3\text{PS}_4$  were introduced inside the die-set on top of the lithium disk, and pressed by hydraulic press (YL-24, MTI Corp.) at 2 MPa to form a prepellet. Afterward, another lithium disk was placed over the electrolyte prepellet. The preformed cell was finally pressed at 10 MPa for 1 min, at 20 °C, using the hydraulic press. The pressure in the cells during the measurements is kept constant by using a torque wrench. The same cell setup and assembly was used for all-solid-state cells except that instead of the second lithium foil in case of symmetric lithium cells, the cathode composite powder was carefully spread on the solid electrolyte layer and pressed at

10 MPa for 1 min. Ionic conductivity measurement was conducted using stainless steel, In, or carbon cloth as blocking electrodes in a torque cell utilizing a Solartron SI 1260 impedance/gain phase analyzer from 1 MHz to 0.05 Hz at an AC amplitude of 10 mV.

### Acknowledgements

Open access funding enabled and organized by Projekt DEAL.

### Conflict of Interest

The authors declare no conflict of interest.

### Data Availability Statement

Research data are not shared.

### Keywords

inorganic solid electrolytes, glassy sulfide, lithium metal, LiI-doped LPS, solid-state batteries

Received: May 10, 2021

Revised: June 14, 2021

Published online: July 10, 2021

- [1] a) M. A. J.-M. Tarascon, *Nature* **2001**, *414*, 359; b) A. Manthiram, X. Yu, S. Wang, *Nat. Rev. Mater.* **2017**, *2*, 16103.
- [2] a) M. Onuki, S. Kinoshita, Y. Sakata, M. Yanagidate, Y. Otake, M. Ue, M. Deguchi, *J. Electrochem. Soc.* **2008**, *155*, A794; b) E. Quartarone, P. Mustarelli, *Chem. Soc. Rev.* **2011**, *40*, 2525.
- [3] J. C. Bachman, S. Muy, A. Grimaud, H.-H. Chang, N. Pour, S. F. Lux, O. Paschos, F. Maglia, S. Lupart, P. Lamp, L. Giordano, Y. Shao-Horn, *Chem. Rev.* **2016**, *116*, 140.
- [4] Y. Kato, S. Hori, T. Saito, K. Suzuki, M. Hirayama, A. Mitsui, M. Yonemura, H. Iba, R. Kanno, *Nat. Energy* **2016**, *1*, 16030.
- [5] Q. Zhang, D. Cao, Y. Ma, A. Natan, P. Aurora, H. Zhu, *Adv. Mater.* **2019**, *31*, 1901131.
- [6] R. Kanno, M. Murayama, *J. Electrochem. Soc.* **2001**, *148*, A742.
- [7] a) Z. Liu, W. Fu, E. A. Payzant, X. Yu, Z. Wu, N. J. Dudney, J. Kiggans, K. Hong, A. J. Rondinone, C. Liang, *J. Am. Chem. Soc.* **2013**, *135*, 975; b) Y. Seino, T. Ota, K. Takada, A. Hayashi, M. Tatsumisago, *Energy Environ. Sci.* **2014**, *7*, 627; c) Ö. U. Kudu, T. Famprikis, B. Fleutot, M.-D. Braid, T. Le Mercier, M. S. Islam, C. Masquelier, *J. Power Sources* **2018**, *407*, 31.
- [8] Y. Zhu, X. He, Y. Mo, *ACS Appl. Mater. Interfaces* **2015**, *7*, 23685.
- [9] J. D. Wicks, L. Börjesson, G. Bushnell-Wye, W. S. Howells, R. L. McGreevy, *Phys. Rev. Lett.* **1995**, *74*, 726.
- [10] a) E. Rangasamy, Z. Liu, M. Gobet, K. Pilar, G. Sahu, W. Zhou, H. Wu, S. Greenbaum, C. Liang, *J. Am. Chem. Soc.* **2015**, *137*, 1384; b) S. J. Sedlmaier, S. Indris, C. Dietrich, M. Yavuz, C. Dräger, F. von Seggern, H. Sommer, J. Janek, *Chem. Mater.* **2017**, *29*, 1830; c) S.-J. Choi, S.-H. Lee, Y.-C. Ha, J.-H. Yu, C.-H. Doh, Y. Lee, J.-W. Park, S.-M. Lee, H.-C. Shin, *J. Electrochem. Soc.* **2018**, *165*, A957; d) F. Han, J. Yue, X. Zhu, C. Wang, *Adv. Energy Mater.* **2018**, *8*, 1703644; e) S. Spannenberger, V. Miß, E. Klotz, J. Kettner, M. Cronau, A. Ramanayagam, F. di Capua,

- M. Elsayed, R. Krause-Rehberg, M. Vogel, B. Roling, *Solid State Ionics* **2019**, *341*, 115040.
- [11] T. Kimura, A. Kato, C. Hotehama, A. Sakuda, A. Hayashi, M. Tatsumisago, *Solid State Ionics* **2019**, *333*, 45.
- [12] A. Hayashi, A. Sakuda, M. Tatsumisago, *Front. Energy Res.* **2016**, *4*.
- [13] D. H. Kim, D. Y. Oh, K. H. Park, Y. E. Choi, Y. J. Nam, H. A. Lee, S.-M. Lee, Y. S. Jung, *Nano Lett.* **2017**, *17*, 3013.
- [14] a) N. H. H. Phuc, E. Hirahara, K. Morikawa, H. Muto, A. Matsuda, *J. Power Sources* **2017**, *365*, 7; b) N. H. H. Phuc, T. Yamamoto, H. Muto, A. Matsuda, *Inorg. Chem. Front.* **2017**, *4*, 1660.
- [15] S. Ito, M. Nakakita, Y. Aihara, T. Uehara, N. Machida, *J. Power Sources* **2014**, *271*, 342.
- [16] a) D. A. Ziolkowska, W. Arnold, T. Druffel, M. Sunkara, H. Wang, *ACS Appl. Mater. Interfaces* **2019**, *11*, 6015; b) D. Y. Oh, A. R. Ha, J. E. Lee, S. H. Jung, G. Jeong, W. Cho, K. S. Kim, Y. S. Jung, *ChemSusChem* **2020**, *13*, 146.
- [17] a) Y. Aihara, S. Ito, R. Omoda, T. Yamada, S. Fujiki, T. Watanabe, Y. Park, S. Doo, *Front. Energy Res.* **2016**, *4*; b) Y.-G. Lee, S. Fujiki, C. Jung, N. Suzuki, N. Yashiro, R. Omoda, D.-S. Ko, T. Shiratsuchi, T. Sugimoto, S. Ryu, J. H. Ku, T. Watanabe, Y. Park, Y. Aihara, D. Im, I. T. Han, *Nat. Energy* **2020**, *5*, 299.
- [18] a) C. Yu, S. Ganapathy, J. Hageman, L. van Eijck, E. R. H. van Eck, L. Zhang, T. Schwietert, S. Basak, E. M. Kelder, M. Wagemaker, *ACS Appl. Mater. Interfaces* **2018**, *10*, 33296; b) L. Zhou, K.-H. Park, X. Sun, F. Lalère, T. Adermann, P. Hartmann, L. F. Nazar, *ACS Energy Lett.* **2019**, *4*, 265.
- [19] X. Feng, P.-H. Chien, S. Patel, J. Zheng, M. Immediato-Scuotto, Y. Xin, I. Hung, Z. Gan, Y.-Y. Hu, *Energy Storage Mater.* **2019**, *22*, 397.
- [20] M. Calpa, N. C. Rosero-Navarro, A. Miura, K. Tadanaga, *Inorg. Chem. Front.* **2018**, *5*, 501.
- [21] T. Shi, Q. Tu, Y. Tian, Y. Xiao, L. J. Miara, O. Kononova, G. Ceder, *Adv. Energy Mater.* **2020**, *10*, 1902881.
- [22] a) M. J. Wang, R. Choudhury, J. Sakamoto, *Joule* **2019**, *3*, 2165; b) E. Kazyak, R. Garcia-Mendez, W. S. LePage, A. Sharafi, A. L. Davis, A. J. Sanchez, K.-H. Chen, C. Haslam, J. Sakamoto, N. P. Dasgupta, *Matter* **2020**, *2*, 1025.
- [23] S. K. Wladislaw Waag, D. Uwe Sauer, *Appl. Energy* **2013**, *102*, 885.
- [24] a) J. Y. Song, H. H. Lee, Y. Y. Wang, C. C. Wan, *J. Power Sources* **2002**, *111*, 255; b) S. Wenzel, D. A. Weber, T. Leichtweiss, M. R. Busche, J. Sann, J. Janek, *Solid State Ionics* **2016**, *286*, 24.
- [25] K. Kerman, A. Luntz, V. Viswanathan, Y.-M. Chiang, Z. Chen, *J. Electrochem. Soc.* **2017**, *164*, A1731.
- [26] a) U. Ulissi, I. Seitaro, H. S. Milad, V. Alberto, A. Yuichi, P. Stefano, *Adv. Energy Mater.* **2018**, 1801462; b) S. M. Hosseini, A. Varzi, S. Ito, Y. Aihara, S. Passerini, *Energy Storage Mater.* **2020**, *27*, 61.
- [27] A. L. Santhosha, N. Nazer, R. Koerver, S. Randau, F. H. Richter, D. A. Weber, J. Kulisch, T. Adermann, J. Janek, P. Adelhelm, *Adv. Energy Mater.* **2020**, *10*, 2002394.